Journal of Environmental Chemical Engineering 10 (2022) 107456

Contents lists available at ScienceDirect

Journal of Environmental Chemical Engineering

journal homepage: www.elsevier.com/locate/jece

Characterization of humic substances isolated from a tropical zone and their role in membrane fouling

M.A.C.K. Hansima [a], A.T. Jayaweera [b], J. Ketharani [c], Tharindu Ritigala [d], Libing Zheng [d], D. R. Samarajeewa [c,*], K.G.N. Nanayakkara [c], Ajith C. Herath [e], Madhubhashini Makehelwala [f], K.B. S.N. Jinadasa [c], S.K. Weragoda [b,f], Yuansong Wei [d,g], Rohan Weerasooriya [g,*]

[a] Postgraduate Institute of Science (PGIS), University of Peradeniya, Sri Lanka
[b] National Water Supply and Drainage Board, Katugastota 20800, Sri Lanka
[c] Department of Civil Engineering, Faculty of Engineering, University of Peradeniya, Sri Lanka
[d] Department of Water Pollution Control Technology, Research Centre for Eco-Environmental Sciences, Chinese Academy of Sciences, Beijing 100085, China
[e] Department of Chemical Sciences, Faculty of Applied Sciences, Rajarata University of Sri Lanka, Sri Lanka
[f] China Sri Lanka Joint Research and Demonstration Centre for Water Technology, Ministry of Water Supply, E.O.E Pereira Mawatha, Meewathura, Peradeniya 20400, Sri Lanka
[g] National Institute of Fundamental Studies, Kandy 20000, Sri Lanka

ARTICLE INFO

Editor: Xiwang Zhang

Keywords:
Sri Lanka
Humic acid
Fulvic acid
EDR
Membrane fouling mechanisms

ABSTRACT

Humic substances (HS) are heterogeneous organic polymers that show monotonous properties. HS are present at different proportions in the terrestrial environment, and they implicate the performance of water desalination plants. Recently electrodialysis self-reversal (EDR) technology has been used to treat excess salinity, hardness and fluoride in HS rich groundwater in Sri Lanka (~3 mg L^{-1}, dissolved C). Due to the high organic content of HS in groundwater, the EDR ion exchange membranes are prone to fouling. To unravel the fouling mechanisms, humic acid (HA) and fulvic acid (FA) fractions were isolated and fractionated from the groundwater and characterized spectroscopically. All membrane fouling experiments were conducted for HA and FA contaminated water using a lab-scale EDR setup operated under batch mode. Sequential desorption experiments were carried out using distilled water, 2% (w/w) NaCl, and 0.3% (w/w) sodium dodecyl sulfate to probe variations among two fouling mechanisms. Similarities were found in aromatic and aliphatic carbon contents, humification degree, and molecular weight of humic substances. Higher proportions of carboxylic and phenolic groups were found in FA compared to HA. Ester groups in HA facilitate P, S, and Si migration within organic moieties. The molecular environs in the vicinity of carboxyl functional groups led different fouling mechanisms. HA fouling was found irreversible compared to FA fouling. The subtle differences between fouling mechanisms will help implement appropriate pretreatments to ensure the durability of EDR membranes.

1. Introduction

Natural organic matter is ubiquitous, showing a monotonous structural framework despite its geographic diversity. Humic substances (HS) included in natural organic matter are heterogeneous, recalcitrant biomolecules derived from intense humification and pose high to moderate molecular weights (500–100 000 Da). Three fractions are operationally defined according to HS acid and base solubility, a) low molecular weight (1 000–10 000 Da) fulvic acid, FA, soluble at any pH), b) high molecular weight (10 000–100 000 Da) humic acid, HA, a soluble fraction above pH 2), and c) humins (100 000–10 000 000 Da), water-insoluble fraction [1]. The composition of major elements in HA and FA are ranged as C (40–60%), H (4–5%), N (1–4%), O (30–50%), S (1–2%), P (0–0.3%) regardless of their source, or degree of humification [2]. However, the oxygen content is high in FA while C, H, N and S contents are high in HA. Distinct functional groups in HS are carboxylic, phenolic, aliphatic, hetero-aliphatic acetal, carbonyl, and their aromatic/ aliphatic skeletons are crosslinked by O and N derived heteroatoms [3]. Solubility of FAs at any pH is associated with their high proportions of carboxyl, phenolic and ketonic surface functionalities

* Corresponding authors.
E-mail addresses: dinushi.s@eng.pdn.ac.lk (D.R. Samarajeewa), rohan.we@nifs.ac.lk (R. Weerasooriya).

https://doi.org/10.1016/j.jece.2022.107456
Received 20 November 2021; Received in revised form 28 January 2022; Accepted 21 February 2022
Available online 23 February 2022

compared to HAs.

HS is also a surfactant capable of interacting with both hydrophobic and hydrophilic contaminants present in the environment [4]. Another important aspect of HS is their ability to formulate organo-complexes with inorganic anions (i.e., phosphate, sulfate, and silicate) and cations by various complexation mechanisms. For example, He et al. (2006) reported probable HS bound P forms as orthophosphate, orthophosphate monoesters, orthophosphate diesters, and phosphonates [5] while others noted phosphate binding to HS using multivalent metal ion bridges to form HS-metal-phosphate complexes [6–8]. Silica included organo-silicate esters with HS accounted for transportation and dissolution in natural aquatic systems [9]. Sulfur present in HS can either be as thiol, thiophene, sulfoxide, sulfone, disulfides, and sulfonate or sulfate esters [1]. Also observed is enhanced Ca^{2+} complexation by sulfonates in groundwater HS [10]. Aquatic or soil HS in non-tropical regions of the world suggests that HAs posture aromatic skeletons, while FAs are aliphatic [11–15].

Conventional experimental methods cannot resolve subtleties inherent in humic substances' fine molecular structures. HS are precursor of forming potential toxicants in water [2,3,16,17]; however, no water regulatory guidelines have been imposed yet for its control. One cannot obtain natural organic matter devoid of water; therefore, keeping its concentration below a threshold level is the only viable option to minimize suspected health effects and prevent membrane fouling.

Further, natural water in the tropics contains high dissolved natural organic matter concentrations compared to temperate regions [18]. Fluctuating soil water profile due to frequent and high levels of rainfall inherited in the tropics facilitates the loading of natural organic matter to shallow groundwater through vertical leaching from near soil surfaces [18]. Therefore, desalination membrane plants used in the tropics often observe fouled membranes due to high dissolved natural organic matter and TDS [1,19–21]. Both pressure-driven (e.g., reverse osmosis, nanofiltration) and ion exchange membranes (i.e., electrodialysis) are used in water desalination. The pressure-driven membrane methods desalinate water excessively that require artificial solutes additions to the treated water [22]. Electrodialysis methods can regulate water salinity cost-effectively [20]. However, in both cases, membrane fouling by natural organic matter and microorganisms is a pressing problem that requires urgent attention [19].

Presently, we focused on examining the fouling of ion-exchange membranes (IEMs) used in electrodialysis self-reversal (EDR) systems by HS in groundwater. It can affect process parameters like power consumption, water recovery, maintenance, and robustness to inlet water quality variations. IEMs bear a net electrical charge, either positive (anion exchange membrane, AEM) or negative (cation exchange membrane, CEM). The natural water contains colloids, natural organic matter, and divalent cations, which show membrane fouling at different proportions. The membrane fouling caused by divalent cations, colloids, or organisms can be removed during the self-cleaning mechanisms using purging and scalants dissolution as employed in EDR [20]. However, the membrane fouling created by HS or allied ternary complexes does not remove efficiently by the self-cleaning process [23]. Therefore, natural organic matter fouled membranes deteriorate their performance due to the formation of organic gels on the surface. Often permanent damage to the membrane could occur, which requires its replacement. IEM fouling by phenols [24], proteins [25,26], tannins [27], natural organic matter [28], antibiotics [29], and anti-foaming agents [30] has widely been examined and relevant mechanisms include precipitation, complexation, and aggregation reactions as discussed elsewhere [20]. However, the relevant fouling mechanisms were mostly speculative; in some cases, no experimental evidence is shown [20].

This study focuses on identifying subtle differences in IEM-fouling mechanisms due to structural variations inherited in groundwater HA and FA due to humification. Fouling mechanisms are supported by the structural composition gained by HS characterization; in-depth characterization of fouled membranes by vibrational spectroscopy was carried out to assess the reversibility or irreversibility of the foulants by sequential desorption experiments. Even though literature reports certain IEM fouling data due to HS [28,31], there is not much research carried out to probe fouling mechanisms comprehensively by considering HA and FA separately.

Therefore, we examined the fouling mechanism of AEM by HS received from a tropical zone in Sri Lanka by spectroscopic and conventional experimental methods. We extracted and fractionated HS in groundwater collected from Sri Lanka. The isolated HS fractions were characterized by attenuated total reflection-Fourier transform infrared (ATR-FTIR), UV-Visible, and X-ray photon (XPS) spectroscopy. Fouling mechanisms of AEM by HS were examined using a batch mode EDR system. Both CEM and HS are negatively charged at natural water acidity; therefore, repulsive electrostatic forces inhibit HS and CEM intimate interactions. CEM fouling by HS is hypothesized minimal, and hence not examined. The mechanisms and procedure developed to probe AEM fouling can also be used to identify fouling of nano or reverse osmosis membranes. Further, we also identified spectral signatures to assess the degree of humification required in HS genesis.

2. Materials and methods

2.1. Chemicals

Unless otherwise specified, analytical grade sodium dodecyl sulfate (SDS), NaCl, and $NaHCO_3$ were obtained from Sigma-Aldrich (USA) and used as received. In all sample preparations, distilled water (JP Selecta AC-L4, Greece) was used.

2.2. Fractionation of dissolved humic substances

A 200 L of water sample was collected into acid-washed HDPE cans during the wet climatic season (October-17, 2020) from Padaviya (Sri Lanka), a location mentioned in a previous study where kidney problems are prevalent (latitude 8°51'04.6", 80°45'00.6", Padaviya, Northcentral province (NCP), Sri Lanka) [17]. Water quality parameters were summarized in Table 1-S (support documentation). According to Thurman and Malcolm, HA and FA were extracted using XAD-8 resin [32]. The resin was first rinsed with methanol, followed by distilled water until removal of traces of methanol, and secondly with 0.1 N NaOH, followed by complete removal of NaOH by rinsing with distilled water. The resin was packed in a 500 mL bed volume glass column. The pre-filtered sample was adjusted to pH 2.0 and passed through the column upward. HS fraction was eluted with 0.1 N NaOH in the reverse direction, and the eluted sample was then re-concentrated in a cleaned small XAD-8 column (160 mL, bed volume). Eluted sample from the second column was fractionated by adjusting pH to 1.0. HA and FA fractions were separated from the settled sample by centrifugation. Re-concentration of supernatant FA fraction and removal of excess HCl from HA precipitate was followed by a hydrogen saturation step through cleaned cation exchange resin. The extraction and fractionation process are detailed in Table 2-S.

2.3. Analytical methods for analysis of humic substance

2.3.1. Dissolved organic carbon content

Dissolved organic carbon (DOC) contents were determined by a total organic carbon analyzer (TOC-L, Shimadzu, Japan). Potassium hydrogen phthalate standard ranging from 0 to 20 mg L^{-1} was used to calibrate total carbon content (TC), while inorganic carbon content (IC) was calibrated by sodium carbonate standard ranging from 0 to 200 mg L^{-1}.

2.3.2. ATR-FTIR spectroscopy

Attenuated total reflection-Fourier transform infrared (ATR-FTIR) spectra of humic fractions were recorded over a wavenumber range from

4000 to 400 cm^{-1} by mounting 1 mg of the solid sample on a diamond prism of a sample holder (UATR two, PerkinElmer, USA). Overlapped peaks were resolved using Gaussian fitting function (Origin pro 2018, MicroLabs, USA).

2.3.3. X-ray photoelectron spectroscopy (XPS)

XPS data for extracted HS were acquired using ESCLAB 250Xi spectrophotometer (Thermo Scientific, Germany). All measuring conditions and sample pellets were prepared as shown elsewhere [17]. Survey spectrums of HA and FA fractions were obtained using CasaXPS software, Germany. Overlapped C 1 s, O 1 s, N 1 s, S 2p, and P 2p peak regions were resolved using Shirley background and Lorentzian-Gaussian (G/L = 70/30) peak-fitting function from the same software.

2.3.4. UV-Visible spectroscopy and spectroscopic indexes

UV-Visible spectra of HS were obtained for dissolved samples in 10 mM sodium acetate with acetic acid buffer at pH 7, between 190 and 700 nm by UV-Vis spectrophotometer (Shimadzu UV-2700). Samples were introduced in a quartz cell with a path length of 1 cm. Relative absorbance ratios, E_{253}/ E_{203} (ratio of UV absorbance at 253 nm and 203 nm wavelengths), E_{250}/ E_{365}, E_{270}/ E_{400} and E_{465}/ E_{665} were used to determine the characteristics of HS [33,34]. Specific UV absorbance at 254 nm ($SUVA_{254}$, m mg L^{-1}) was calculated to compare the hydrophobicity of HS [33]. Optical density at 280 nm (ε_{280}, cm mol^{-1} cm^{-1}) (UV absorbance coefficient at 280 nm divided by TOC of the sample) for each sample was also calculated.

2.4. Membrane fouling and desorption

Laboratory scale EDR system (Fig. 1-S: support documentation) contained CJMA-4 (anion membrane) and CJMC-4 (cation membrane) ion-exchange membranes (Hefei ChemJoy Polymer Materials Co., China). Specification of the stack system is summarized in **Table 3-S**. Feed solutions were prepared to simulate groundwater composition. First, HA feed solution was prepared by dissolving 0.0056 ± (0.0001) g of extracted solid sample (~2 mg L^{-1}, TOC) in 1 L of distilled water, and NaCl (0.001 M) and $NaHCO_3$ (0.001 M) was added. The second feed solution containing FA was prepared by dissolving 0.0048 ± (0.0001) g of extracted solid sample (~2 mg L^{-1}, TOC), and salts were added as same as the previous solution. Both feed solutions were adjusted to pH 8.00 (Orion 910003, USA) using 0.1 N NaOH or 0.1 N HCl solutions, stirred overnight, and filtered through 0.45 μm PES membranes before feeding them into the EDR system. Further, the pH of the HS feed and the concentrate solutions were maintained at pH 8.00 during each EDR cycle using 0.1 N NaOH or 0.1 N HCl solutions.

After each fouling experiment, the AEM was dismantled from the EDR stack system to evaluate fouling characteristics by ATR-FTIR (UATR two; PerkinElmer, USA) and SEM (EVO LS 15; ZEISS, Germany) methods. Chemical desorption was carried out first by soaking torn pieces (~0.5 × 0.5 cm^2) from 3.0 × 3.0 cm^2 dried fouled membranes in 100 mL of distilled water with stirring for 24 h. Membranes were taken out and dried in a desiccator. Water desorbed membranes were then soaked in 2% (w/w) NaCl and 0.5% (w/w) SDS separately while stirring for 24 h. Initial and the final pH, EC (conductivity cell probe; Orion 013010MD, USA), DOC content, of desorption solutions were measured. The study was replicated three times.

3. Results and discussion

3.1. Characterization of humic substances

3.1.1. ATR-FTIR spectroscopy

The HS, e.g., FA and HA, were characterized by IR spectroscopy, the spectral regions are grouped as 3600–2200 cm^{-1} (high-frequency region), 1800–1500 cm^{-1} (mid-frequency region), and 1400–400 cm^{-1} (low-frequency region) (Fig. 1) and peaks were identified according to the data [10] available for Sigma-Aldrich humic acid (**Table 4-S**). The spectral signatures specific to FA and HA were analyzed in corroboration with XPS results, as shown in Section 3.1.2. In the high-frequency IR region, the C-H stretching vibrations of FA have resolved into three bands, namely 3052 cm^{-1}, 2922 cm^{-1}, and 2821 cm^{-1}. However, only the band at 2922 cm^{-1} is present for HA. Compared to HA, FA shows enhanced aliphatic [35] and recalcitrant properties [36]. In HA, the band at 3131 cm^{-1} is ascribed to aromatic C-H stretching ($\nu_{(C\text{-}H)\ ar}$), whereas similar signatures in FA are absent or not significant. FA $\nu_{(C\text{-}H)\ ar}$ shows a blueshift of 5 cm^{-1} due to electron attracting phenolic and carboxylic groups in the organic moieties. Both FA and HA show similar spectral features for the H bond and O-H stretching vibrations ($\nu_{(O\text{-}H)}$) due to their hydrophilic nature [36].

In the mid-frequency region, the FA spectrum shows two bands at 1740 cm^{-1} and 1706 cm^{-1} due to C═O stretching vibrations ($\nu_{(C\text{=}O)}$) in -COOH (the XPS data in Fig. 2 shows only a minute proportion of ketonic groups). The $\nu_{(C\text{=}O)}$ band at 1710 cm^{-1} for HA shows lower -COOH, and the higher relative intensity of $\nu_{(C\text{=}C)\ ar}$ stretching band at 1623 shows a high proportion of aromatic carbon. Relative abundance of -COOH groups in FA compared to HA is supported by a broadband for asymmetric COO^- stretch ($\nu_{(COO\text{-})\ asym}$) at 1535 cm^{-1}. As shown in Fig. 1. **c** and **1. f**, the spectral evidence in low-frequency range has resolved into CH_2/ CH_3 deformations ($\nu_{(C\text{-}H)\ def}$), an asymmetric stretch of COO^- ($\nu_{(COO\text{-})\ sym}$), aromatic C-O-H stretch ($\nu_{(C\text{-}O\text{-}H)\ ar}$), an antisymmetric stretch of COO^- ($\nu_{(COO\text{-})\ asym}$), O-H bend of COOH/ phenol ($\nu_{(O\text{-}H)\ bend}$), R-O stretching of alkoxy groups (R-OR, R-OH, and carbohydrates) ($\nu_{(R\text{-}O)}$), C-O stretch of esters ($\nu_{(C\text{-}O)}$), aliphatic alcoholic O-H deformation ($\nu_{(R\text{-}O\text{-}H)\ def}$), phenolic O-H deformation ($\nu_{(C\text{-}O\text{-}H)\ ar}$) and aromatic C-H deformation ($\nu_{(C\text{-}H)\ def\ ar}$). In the current study, FA and HA display $\nu_{(C\text{-}H)\ def}$ bands at 1445 cm^{-1} and 1455 cm^{-1}. Aliphatic and aromatic -OH deformations resolved in HA and FA as shown in Fig. 1. The $\nu_{(R\text{-}O\text{-}H)\ def}$ of HA at 1419 cm^{-1} is broad (the corresponding band at 1455 cm^{-1} of FA is narrowed), indicating high aliphatic -OH groups in HA. However, the phenolic content in FA is more abundant than in HA. The well-resolved band ($\nu_{(C\text{-}O)}$) at 1259 cm^{-1} in HA is ascribed to the ester group in HA (such groups are absent in FA). The linkages evidenced for the presence of organo-silicate and organo-sulfate ester as further supported by XPS data (Fig. 2). The -O-H bending vibrations in -COOH at is broader in FA ($\nu_{(O\text{-}H)\ bend}$ 1201 cm^{-1}) compared to HA ($\nu_{(O\text{-}H)\ bend}$ 1215 cm^{-1}). The HA shows a narrow, intense band corresponding to alkoxy groups, $\nu_{(R\text{-}O)}$ at 1090 cm^{-1}, while the FA shows a cluster of bands in the 1119–1040 cm^{-1} region. Further, the appearance of vibration bands within 1100–1000 cm^{-1} [5] could also be due to mono- and/ or di-ester-phosphate groups in the HS. Therefore, due to ester bonded phosphate, the band assigned as $\nu_{(R\text{-}O)}$ at 1090 cm^{-1} in the HA can also be assigned. The $\nu_{(R\text{-}O\text{-}H)\ def}$ stretches were identified for each fraction for HA at 1032 cm^{-1} and FA at 967 cm^{-1}. The band at 853 cm^{-1} appeared only in the HA spectrum attributes Si-O stretching ($\nu_{(Si\text{-}O)}$) of silica and was found as another proof of the higher amount of humic complexed silica observed in the XPS survey data. Vibrational peaks > 600 cm^{-1} are attributed to mineral matter associated with HS.

3.1.2. XPS spectral data

XPS analysis is extremely sensitive to near-surface features, and thus used to determine the elemental composition of a substance, semi-quantitatively. However, inaccuracies may result if the material is heterogeneous, and surface chemical composition is differed from the bulk [37]. According to the XPS survey spectra, the HA (Fig. 2a) and the FA (Fig. 2b) fractions consist with C, O, Si, Cl, N and S as major elements along with traces of Ca, Na, Mg and P. The abundance of elements in HA follows C 1 s (66.36%) < O 1 s (21.24%) < Si 2p (6.75%) < Cl 2p (1.95%) < N 1 s (1.71%) < S 2p (0.87%) < Na (0.74%) < Ca 2p (0.32%) and for the FA fraction as C 1 s (71.42%) < O 1 s (22.87%) < Cl 2p (1.64%) < N 1 s (1.57%) < S 2p (0.98%) < Si 2p (0.71%) < Na (0.50%) < Ca 2p (0.12%) < P 2p (0.11%) < Mg 1 s (0.09%). The abundance of O

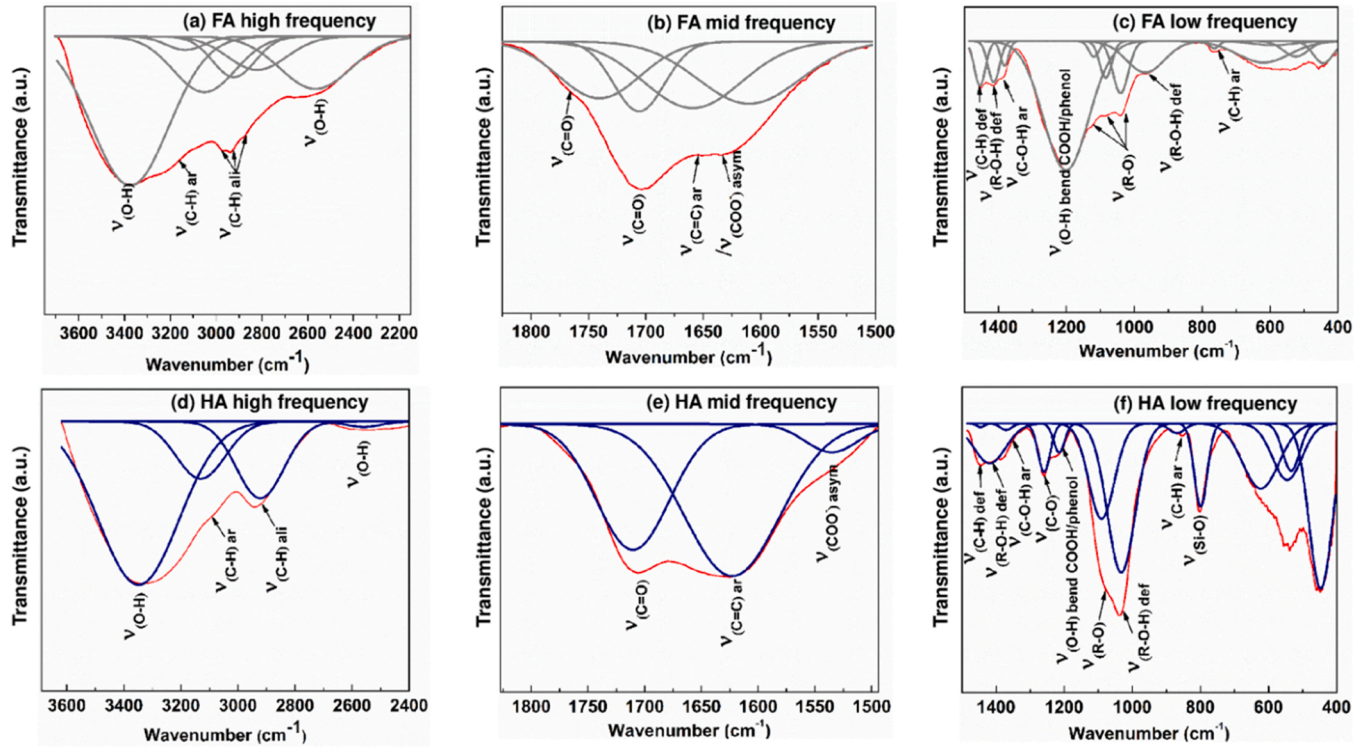

Fig. 1. ATR-FTIR spectral data of fulvic and humic acids a) FA 3600–2200 cm^{-1}, b) FA 1800–1500 cm^{-1}, c) FA 1300–400 cm^{-1}, d) HA 3600–2200 cm^{-1} e) HA 1800–1500 cm^{-1}, f) HA 1300–400 cm^{-1}.

and N derived functionalities on HA and FA can be postulated by O/C and N/C elemental ratios. These elemental ratios in commercial Sigma-Aldrich and Sri Lankan HA are comparable; O/C 0.32 (Sri Lankan HA), 0.33 commercial HS; N/C 0.026 (Sri Lankan HA) and 0.021 commercial HS [10,38]. Binding energies (BEs) and abundance of assigned status are summarized in **Table 5-S**. Notably as shown in Table 1, carbon content and aromaticity of the HS in groundwater from tropical zone (Sri Lanka) are highest.

3.1.2.1. C1 s–chemical state. As shown in Fig. 2**a** and **b**, the C 1 s deconvoluted spectra for HA and FA show six peaks designated as (1) sp^2 hybridized aromatic carbon (C-C/C-H), (2) sp^3 hybridized aliphatic carbon (C-C/C-H), (3) α-carbon (α-C-C(O)), (4) alcohol/ether carbon (C-O), (5) ketonic carbon (C═O), and (6) carboxylic carbon (C-(O)O)[10, 39]. Further, the π-π * shake-up satellite peak that appears at ~291 eV was not resolved. For Sri Lankan HS, the aromatic carbon content of HA (54.09%) was higher than FA (52.51%), while aliphatic carbon content was higher for FA (3.34%) than for HA (2.28%). The HA extracted from groundwater in CKDu zones show higher aromaticity for HA than FA. The π-π * shake-up satellite peak indicates aromaticity [40]. Accordingly, HA exhibits a more aromatic nature than FA. The most abundant C 1 s state consists of either/alcohol carbon, and their composition is higher for HA (31.33%) than FA (27.20%). In agreement with FTIR data, the higher surface carboxylic content appeared in the FA (11.70%) than in HA (6.37%). The presence of -COOH groups dominates the surface charge of the HS, and it promotes membrane fouling. Phenolic content is also pivotal as the carboxylic content when determining fouling mechanisms. However, XPS data alone cannot resolve the presence of phenolic groups from the alcohol/ether carbon unambiguously because of subtle variations in their BEs [37]. The ketonic carbon content and α-carbon contents are similar in HA and FA.

3.1.2.2. O 1 s–chemical state. De-convoluted O 1 s spectra show four peaks for HA and FA as in Fig. 2**a** and **b**. Peaks can be assigned as (1) carbonyl (O═C), (2) alcohol/acetal/hemiacetal (O-C), (3) carboxylic (C-O-O-H), and (4) ester (O═C-O) oxygen. Carboxylic groups are the most dominant O-containing functionality found in extracted HS, where the amount found in the FA is higher as 91.34% and for the HA as 85.42%. Comparatively higher carboxylic content was found in FA in agreement with C 1 s data. The dominance of the O-containing groups for the HA follows as C-O-O-H > O═C > O-C > O═C-O, while for the FA as C-O-O-H > O-C > O═C > O═C-O. In agreement with vibration spectroscopic data, organo-silicate and sulfates show high ester-type O content in HS. However, the presence of aromatic and aliphatic -OH groups in HS cannot be resolved by XPS data but by IR spectral signature. Accordingly, FA is enriched with aromatic -OH groups [37].

3.1.2.3. N 1 s–chemical state. De-convoluted N 1 s XPS data for the HA fraction and FA fractions are given in Fig. 2**a** and **b**, respectively. Typical N 1 s spectra contained (1) amide (C(O)N), (2) pyrrole (N-pyrrole), and (3) primary amine (NH_2) or protonated primary amine ($^+NH_3$) nitrogen peaks [38,41]. The amide and the pyrrole N 1 s peaks are not resolved well [38]. The FA amide and pyrrole peaks are overlapped, but HA peaks are de-convoluted. The most abundant N-containing group in HA is amide-N (78.29% of total N). The amide-N is predominant in HS over heterocyclic N and ammonium-N [42], resulting from peptides [41]. Peptide bonding and nucleophilic additions with aromatic amines followed by an elimination are possible reaction mechanisms in amide formation in HS-genesis pathways [43]. N-content of the HA vary as amide (78.29%) > pyrrole (19.65%) > amine (2.06%). The least amine contents in HS indicate its recalcitrant nature due to intense humification [41]. For FA, primary amine N (60.7%) is higher than amide/pyrrole N (39.3%), indicating enhanced proportions of peptides and proteins held by H-bonding [44]. However, our HS does not contain aromatic-N (pyridine, imine, aniline), where they show typical BE at 399.0 eV [44]. Therefore, protein/peptide nitrogen content determines the N content of extracted HS.

3.1.3. Organic complexes of sulfate, silicate, and phosphate

Complex formation between sulfate, silica, phosphate, and HS in

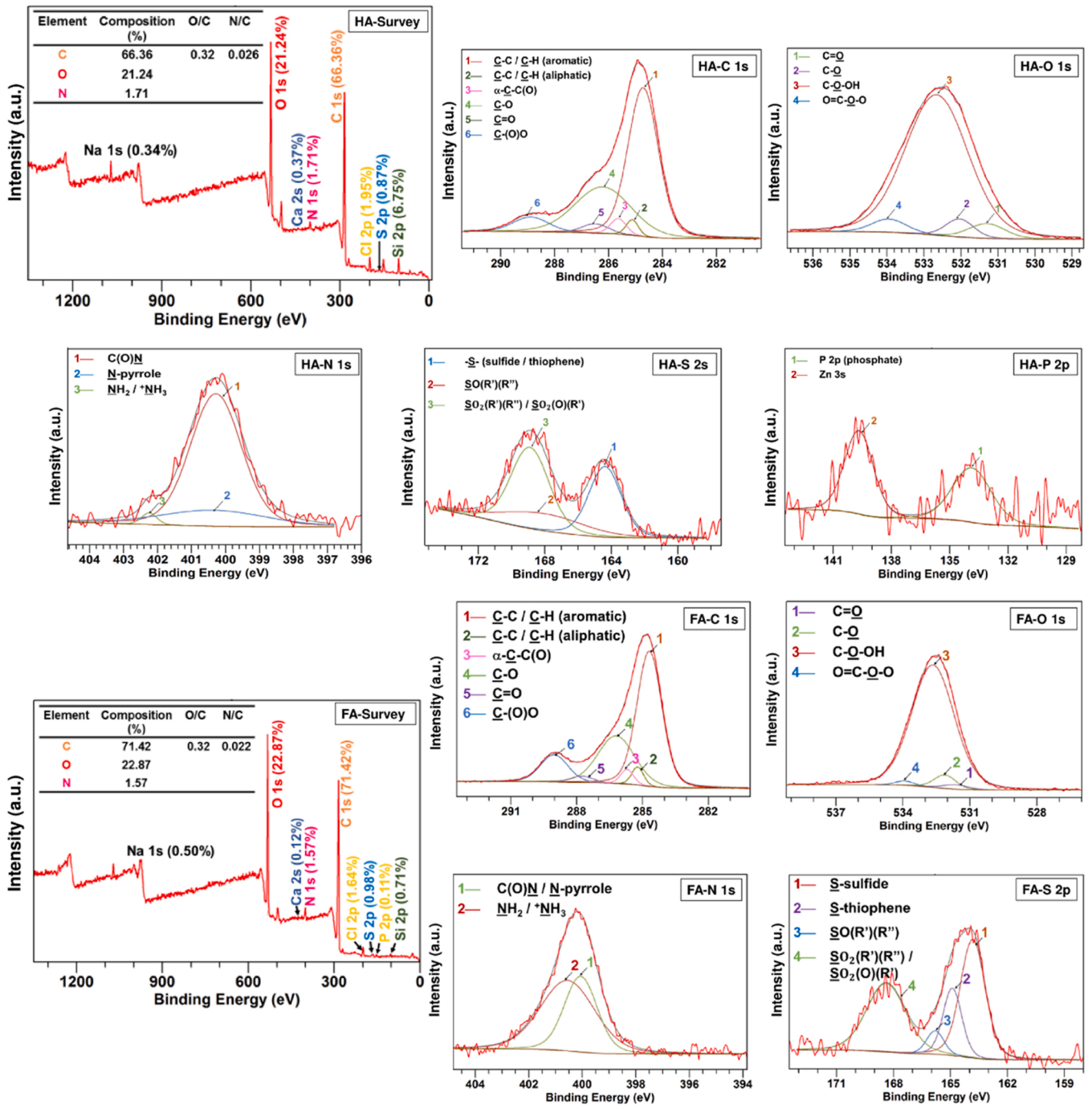

Fig. 2. Fig.2.a: XPS spectral data of humic acid fraction including HA-survey spectrum, HA-C 1s status, HA-O 1s status, HA-N 1s status, HA-N 1s status, and HA-P 2p status. Fig. 2.**b:** XPS spectral data of fulvic acid fraction including FA-survey spectrum, FA-C 1s status, FA-O 1s status, FA-N 1s status, and FA-S 2p status,.

natural aquifers have been studied extensively [45,46,6–8]. Further, the complexation mechanisms are believed to be mediated by multivalent metal ions in soils or water through bridging interactions [6,8,47]. Both HA and the FA show surface-bound S, Si, and P, which favors bridging interactions with Al^{3+}, Fe^{2+}, $Ca^{2+,}$ and Mg^{2+}.

3.1.3.1. S 2p–chemical state. Lorentzian-Gaussian fitted S 2p XPS curves are shown for HA and FA in Fig. 2**a** and **b** respectively, and corresponding BEs were summarized with their relative abundance in **Table 5-S**. Four peaks are identified for FA as (1) sulfide, (2) thiophene, (3) sulfoxide (SO(R')(R'')), and (4) sulfone (SO_2(R')(R'')) or ester-bonded sulfate (SO_2(O)(R'')). However, there are only three peaks for the HA due to sulfide, and thiophene S 2p peaks overlap. Percent compositions of S-containing groups were different among the two fractions. The FA the S 2p composition varies as sulfide (41.41%) > sulfone/ester-bonded sulfate (36.76%) > thiophene (17.34%) > sulfoxide (5.52%) while for the HA as sulfone/ester-bonded sulfate (45.50%) > sulfide/thiophene (33.39%) > sulfoxide (21.11%). The formation of O-containing S functional groups, i.e., sulfone/ester-bonded sulfate and sulfoxides, is probably a result of the oxidation of surface sulfur-containing functional groups like sulfides and thiophenes, thus indicating intense humification [38,48]. Further, the ester-bonded sulfate is believed to be a product of the complex formation reaction between inorganic SO_4^{2-} and COO^- [10]. In the groundwater of HS in the study locations, the

Table 1
Composition, abundance, and characteristics of groundwater humic substances extracted from different regions in the world.

Location	Composition			HA: FA ratio	Characteristics			Reference
	C%	N%	O%		aromatic C%	aliphatic C%	carboxyl C%	
Padaviya, Sri Lanka								
HA	66.36	1.71	21.24	1:10	54.09	2.23	6.37	Current study
FA	71.42	1.57	22.87		52.51	3.34	11.70	
Gorleben, Germany								
HA	56.25	1.69	35.80	NA	41	38	8	[15]
FA	57.18	1.14	35.38		23	48	13	
Fuhrberg, Germany								
HA	54.43	1.69	NA	NA	35.4	42.6	19.5	[13]
FA	54.74	1.02	NA		33.3	36.0	22.6	
Danish aquifers								
HA from Fjand	59.00	NA	NA	100:0	51	8	6	[14]
FA from Tuse and Skugen	48.77–50.32	NA	NA	1:34 (Skugen) 4: 58 (Tuse)	14–20	43–52	19–20	
Vejen landfill, Denmark								
HA	50.7	2.2	42.1	11.9:43.5	NA	NA	NA	[12]
FA	51.4	0.9	42.5					
Biscayne groundwater, Colorado								
HA	58.28	3.39	30.14	NA	36	26	23	[11]
FA	55.44	1.77	35.39		39	17	28	

NA – data not available

ester-bound sulfates are high. Further research into the formation mechanisms of ester-bound HS and hard ions (i.e., Ca^{2+}, Mg^{2+}) mobility in water is warranted. Compared to FA, the presence of higher SO_4^{2-} bound HA triggered by Ca^{2+} is ascribed chelation. The enhanced negative charge in FA inhibits SO_4^{2-} due to electrostatic repulsions [10].

3.1.3.2. Si 2p–chemical state. A higher Si content in HA (6.75%) than FA (1.64%) was noted. The Si may be complex with HS in several ways [9]. In one way, > Si-OH groups may form H-bonds with N or O sites on HS [21,47]. Alternatively, hexa-coordinated chelates between catechol and silica are proposed. Si can also associate with HS forming organo-silicate esters. Although not conclusive to date, the formation of organo-esters seems energetically feasible [9]. In the last mechanism, a nucleophilic attack by dicarboxylic acids to silicic acid at neutral pH promotes -C-O-Si formation. However, the enhanced presence of organo-Si enriched HA is unresolved yet.

3.1.3.3. P 2p–chemical state. Identifying spectral signals corresponding to P is quite challenging in HS. For example, the XPS survey HS data virtually show no evidence for the presence of P in HA, but the de-convoluted spectrum shows P 2p signal at 133.86 eV (Fig. 2**a**). Overlapping regions for P 2p with Zn 3 s and Si 2p are significant; in HA, the P signal is shadowed by an intense peak resulting from Si. Thus, overlapping the high Si amount found in the HA resulted in no separate phosphorus peak in the survey spectrum. However, the survey XPS data of the FA reveals traces of P, but the de-convoluted P 2p data shows no recognizable peaks. Transportation of P with HS is due to the formation of phosphate mono- and di- esters which are enzyme-hydrolyzable and

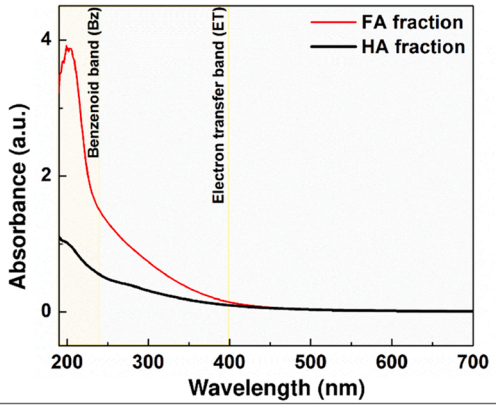

Sample	Spectroscopic indexes					
	E_{ET}/E_{Bz}	ε 280/ L mol^{-1} cm^{-1}	$SUVA_{254}$/ L m^{-1} mg^{-1}	E_{250}/E_{365}	E_{465}/E_{665}	E_{270}/E_{400}
HA	0.48	629.02	8.03	3.96	7.00	4.70
FA	0.33	571.57	6.93	4.85	8.83	7.27
IHSS–HA[a]	0.81	805.50	9.65	2.04	5.30	2.34
IHSS–FA[b]	0.65	474.50	5.00	3.00	13.80	3.50

[a] Mean value of three International Humic Substance Society (IHSS) standard humic acid samples adapted from Fuentes et al. (2006)
[b] Mean value of two International Humic Substance Society (IHSS) standard fulvic acid samples adapted from Fuentes et al. (2006)

Fig. 3. : UV spectroscopic data and calculated spectroscopic indexes for isolated humic and fulvic acids.

acid un-hydrolyzable [34].

Moreover, phosphate binds with HS through metal ions bridging in forming HS-metal-phosphate complexes are also reported [6–8,46]. The detected vibrational peaks correspond to mono- and/or di-ester-phosphate in HA, supporting P 2p state. The absence of the P 2p state in FA suggests weak electrostatic interactions with phosphate, hindering ester linkages require further research.

3.1.4. Ultraviolet (UV) spectroscopy

UV spectral data allow identification of HS humification processes. For HS, three absorption bands are observed: local excitation (LE) band ($\lambda < 190$ nm), benzenoid (Bz) band (λ190–240 nm), and π-π * electron transition (ET) band ($\lambda > 240$ nm) (Fig. 3) [35]. The intensity of the Bz band indicates the HS's aromaticity, while the ET band's position indicates the degree of substituted aromatic constituents [49]. A variety of spectroscopic indexes are introduced to relate the degree of humification and the aromaticity of a HS [35]. This study focused on the ratios of UV absorbance at different wavelengths; viz., 253 nm and 203 nm (E_{ET}/E_{Bz}), at 465 nm and 665 nm (E_{465}/E_{665}), at 250 nm and 365 nm (E_{250}/E_{365}), and at 270 nm and 400 nm (E_{270}/E_{400}). Optical density at 280 nm (ε_{280}) and the specific UV absorbance at 254 nm ($SUVA_{254}$) was also considered.

The E_{ET}/E_{Bz} ratio correlates with the degree of substitutions of O-containing functionalities (i.e., hydroxyl, carbonyl, carboxyl, and ester) to the aromatic ring structure. The E_{ET}/E_{Bz} ratio increases with substituted aromatic constituents in the HS structure. In agreement with XPS data, the E_{ET}/E_{Bz} ratio is higher in HA (0.48) than FA (0.33). Compared to IHSS samples, the degree of humification is less conspicuous in Sri Lankan HS [35]. In agreement with XPS data, the ε_{280} correlates with the HS aromaticity and the molecular weights because of π-π * electron transitions occurring at λ 270–280 nm region [50]. HS contain various subunits such as aniline derivatives, phenolic arenes, polyenes, polycyclic aromatic hydrocarbons, and benzoic acids, responsible for π-π * electron transitions. The ε_{280} values for International Humic Substances Society (IHSS) HAs and FAs suggest higher values for HAs, typically doubled form FAs, indicating higher aromaticity and molecular weights associated with HA fractions. Data obtained from this study denotes minor deviations among their ε_{280} values. Increased aromaticity indicates the degree of humification where condensation of conjugated aromatic and/ or aliphatic structures and inter- or intra-molecular donor-acceptor interactions occur among chromophores forming supramolecular HA or FA aggregates. The $SUVA_{254}$ value has shown a direct relationship with the hydrophobicity of a particular DOC component [51]. Therefore, the $SUVA_{254}$ index is used to assess the hydrophobicity of HA based on normalized TOC values. The HS with $SUVA_{254}$ values greater than 4.0 is said hydrophobic due to their high aromatic nature; thus, HA ($SUVA_{254}$; 8.03) and FA ($SUVA_{254}$; 6.93) show hydrophobic behavior. The hydrophobic nature of HS plays a role in membrane fouling by inter-molecular interactions (Section 3.1.5). Generally, despite some controversies, HS E_{465}/E_{665} ratios correlate with molecular weight, aromatic condensation, and humification [35]. As judged by E_{465}/E_{665} ratios, aromaticity favors HS humification. In humified HS with high molecular weights has E_{465}/E_{665} ratio ranging from 3.0 to 5.0 while young, aliphatic-aromatic, light molecular weight HS show E_{465}/E_{665} ratios ranging from 6 to 10 [52]. The E_{465}/E_{665} index of SL HA (E_{465}/E_{665}; 7.00) is lower than for FA (E_{465}/E_{665}; 8.83). E_{250}/E_{365} index also correlates the aromaticity and molecular weight, given that low values (2.4–3.1) are for aromatic compounds with high molecular weight originated from lignin derivatives [52,53]. Accordingly, Sri Lankan HA and FA belong to light molecular weight fractions with incomplete humification. The E_{270}/E_{400} value correlates with the chromophores' content [50]. In agreement with XPS analysis, our data show that in HS, high carboxyl content is associated with FA structure.

3.2. Postulated membrane fouling mechanisms by humic substances

3.2.1. EDR experimental data

$$D = \frac{\sigma_0 - \sigma_t}{\sigma_0} \times 100 \quad \% \tag{1}$$

$$\text{C loss} = \frac{DOC_i - (DOC_f + DOC_c)}{DOC_I} \times 100 \quad \% \tag{2}$$

Desalination efficiencies, %D of HA and FA feed solutions of EDR batches were calculated according to Eq. 1, where σ_0 and σ_t are electrical conductivity (mS cm^{-1}) at t = 0 and t, respectively in the feed solution and shown in Fig. 4a and b. Gradual deposition of HS foulants on the AEM surface might have enhanced the resistance to mobile ions' movement through the membrane. The steeper decline observed for the desalination rates of HA (HA, from 91.45% to 72.43% within five batches and FA, from 91.35% to 70.67% within seven batches), indicating comparatively high accumulation rate of the foulant on the membrane surface. %Carbon losses in each batch for HA and FA feed solutions were calculated using Eq. 2, where DOC_i, DOC_f, and DOC_c are initial DOC content in the feed water, final DOC content in the feed, and added DOC content in concentrated solution, respectively. Calculated % C loss responsible for the C amount deposited during each EDR batch cycle aided interpretation of foulants' accumulation on the AEM.

Interestingly, the %C content in FA declined from 67.79% to 32.29%, contrary to HA %C content, which increased from 2.85% to 88.71%. Results for FA suggest a higher amount of electrostatic repulsion experienced by the incoming foulants from the foulants already deposited on the AEM surface, validating higher surface negative potential gained by FA due to deprotonation of high quantity of carboxyl and phenolic sites. Surface fouling layers are stabilized due to negative charge neutralization by attracting protons generated from water splitting, as illustrated in the postulated mechanisms (Fig. 6). Electrostatic repulsion in HA is low due to enhanced surface charge neutralization by protonation of the surface carboxyl and phenolic functional groups. The concentration of the ions near the membrane surface has decreased with time, creating an ion deficit interface. At extreme ion deficit conditions, water splitting occurs on the IEM surface generating H^+ and OH^- to facilitate the current flux across the membrane [54,55].

3.2.2. Characteristics of membrane foulants

Deposition of HS has reduced the performance of the AEM. The fouled membrane sites are sensitive to vibration spectroscopic signals. As shown in Fig. 4c and d, IR data was used to postulate HS and membrane interacting mechanisms. Vibrational spectral regions were deconvoluted as detailed in supporting documentation **Figure S-1**. The H-bonded O-H stretching vibrations ($\nu_{(O-H)}$) are observed at 3424 cm^{-1} with a shoulder at 3239 cm^{-1} in the virgin-AEM spectrum. Membrane-foulant interactions resulted in broadening the $\nu_{(O-H)}$ band, and deconvoluted spectra of fouled membranes reveal new peaks, accordingly. These new peaks are probably due to $\nu_{(O-H)}$ of COOH and phenolic groups in FA and HA. Redshifts occurred in the direction of lower wavenumbers to the virgin peak at 3424 cm^{-1} by a $\Delta\nu$, 2 cm^{-1} after HA and by $\Delta\nu$, 20 cm^{-1} after FA fouling suggest H-bonding between water, PVDF-fluorine and carboxyl and/ or phenolic groups in HS [56].

Deconvoluted IR data for the $\nu_{(C-H)}$ region showed additional peaks for aromatic and aliphatic C-H vibrations of HS upon fouling (Fig. 2-S). The aliphatic C-H stretch appeared at 2823 cm^{-1} for FA and 2820 cm^{-1} for HA fouled AEMs and aromatic C-H stretch at 2870 cm^{-1} for FA while at 2884 cm^{-1} for fouled HA. The IR bands of C-H bonds are shifted from the virgin position due to electrostatic and hydrophobic interactions between the membrane and the foulant. The asymmetric stretching vibrations of virgin ^{+}N-C-(CH_3), C-H bond (^{1} $\nu_{(C-H)asym}$) at 3029 cm^{-1} redshifted slightly ($\Delta\nu$, 2 cm^{-1} after HA fouling, $\Delta\nu$, 1 cm^{-1} after FA fouling) due to electrons gained from electrostatic interactions. The

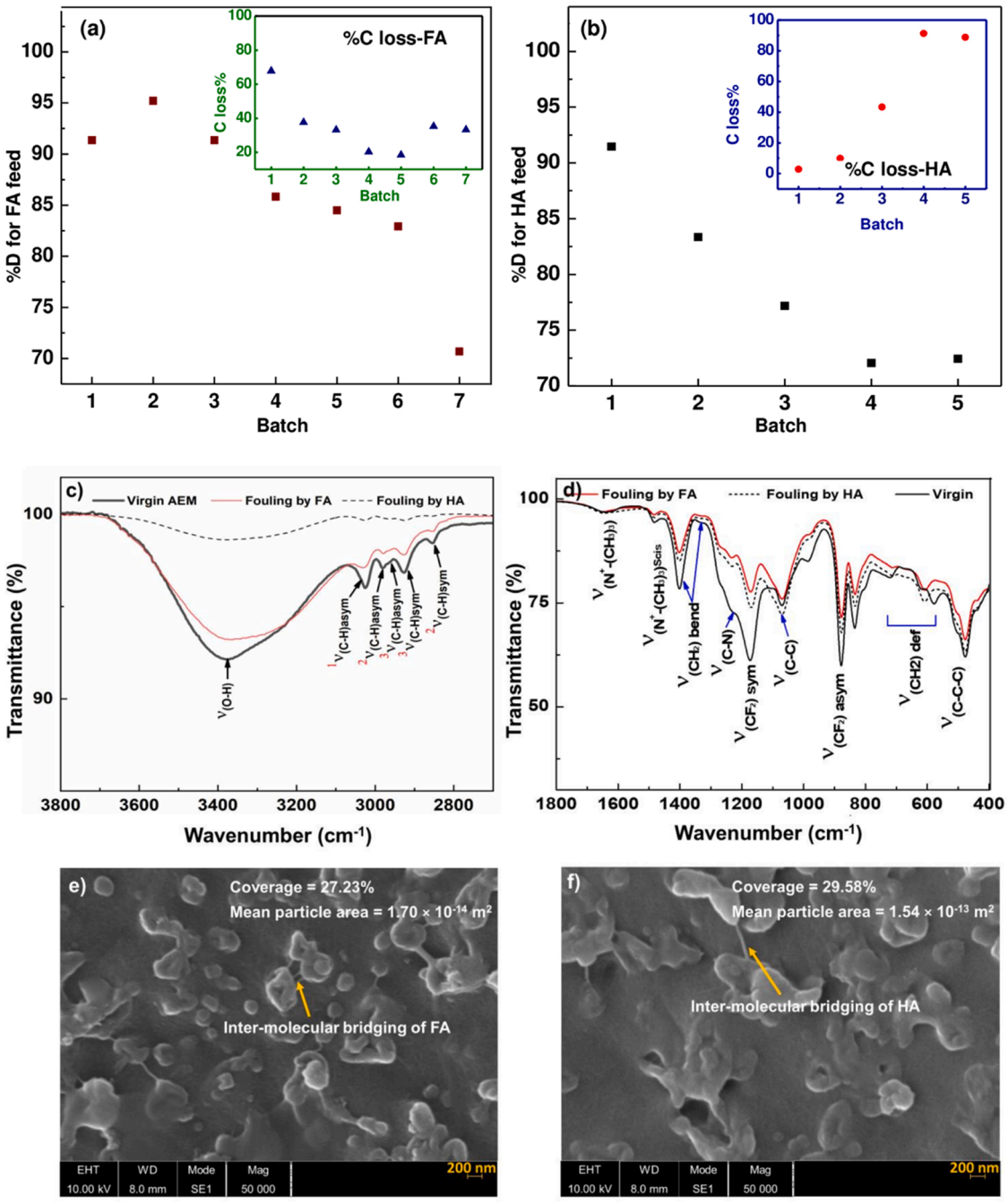

Fig. 4. Variation of desalination efficiency, D% during batch mode EDR cycles along with %C loss for a) FA feed, b) HA feed, ATR-FTIR spectra comparing virgin and fouled EDR-AEMs by fulvic and humic acids c) high-frequency region spectrum (3700–2700 cm^{-1}), d) low-frequency region (1800–400 cm^{-1}) with SEM morphology of e) FA fouled membranes, and f) HA fouled membranes.

asymmetric stretch of CH_2, C-H bond ($^2\nu_{(C\text{-}H)asym}$ at 2963 cm^{-1} blue shifted ($\Delta\nu$, 7 cm^{-1} after HA fouling, $\Delta\nu$, 10 cm^{-1} after FA fouling due to CH-π interactions.

Foulant's double bond features were readily identified from the deconvoluted spectral region for the 1800–1500 cm^{-1} range (Fig. 2-S.a and 2-S.d). Accordingly, aromatic C═C and asymmetric -COO^- stretches are resolved for the HA at 1607–1502 cm^{-1} as sharp peaks while for the FA at 1618–1482 cm^{-1} as broad spectral bands indicate more -COO^- groups in FA structure with the preserved chemical environment. Further, higher carboxyl content in FA was re-confirmed by the appearance of an additional peak at 1713 cm^{-1} due to C═O stretching of -COOH. Virgin vibration peaks correspond to stretching of quaternary ammonium functional sites ($\nu_{(N+\text{-}(CH3)3)}$) at 1642 cm^{-1}, scissoring ($\nu_{(N+\text{-}(CH3)3\ scis)}$) at 1483 cm^{-1} and C-N^+ ($\nu_{(C\text{-}N)}$) stretching at 1231 cm^{-1} blue-shifted upon fouling with HA and FA. Cl^- ions neutralize the positive charge on N functional sites of virgin AEM through electrostatic interactions. As long as fouling by HS might only partially neutralize their positive charge through electrostatic interactions resulted in comparatively high positive nature/ high frequencies, verifying the exchange of Cl^- ions with negative HS.

3.2.3. *Desorption data*

A desorption study was used to disclose the nature of outer and inner reversible foulants detached from the AEM surfaces. The pH of the desorption solutions was affected by the amount of protonated and/or deprotonated carboxyl and phenolic groups presented in the desorbed

HS foulant, and the resulting pH values were summarized in Table 2. Accordingly, DOC_f values obtained during the distilled water desorption evidenced the removal of loosely bound outer HA or FA foulants form on the AEM surface. The final pH of the distilled water was increased after HA or FA desorption, indicating the basic nature of the outer layer foulants. A higher pH increment was observed for FA outer fouling, indicating high carboxylate and phenolate amounts than desorbed HA. Hence, the negative charge of outer foulant layers was deduced as high for FA compared to HA. ATR-FTIR data in Fig. 6 suggest a partial restoration of membrane properties after removal of outer-most FA foulants by distilled water; in contrast, distilled water desorption failed to restore virgin membrane properties for HA fouling. Salt solutions are frequently used to clean the fouled IEMs by organics due to destabilization of membrane-foulant electrostatic interactions [52,53]. Accordingly, 2% (w/w) NaCl used in this study facilitated the desorption of electrostatically bound inner foulants from AEM surface. The final pH of the HA desorbed solution was decreased from the initial pH value of 6.23–5.49, indicating their acidic nature. On the contrary, the pH of the FA desorbed solution was increased to 7.01, indicating their basic nature. This results in line with the idea explained earlier; the protonation of membrane-adhered HA results in neutralized inner fouling layers.

Further, the NaCl desorption was facilitated the partial recovery of the membrane features back to the virgin state for FA, in contrast to deteriorated membranes resulting in HA fouling (Fig. 6). SDS is reported as a surfactant facilitating the removal of hydrophobically attached foulants from membrane surfaces [57]; thus the nature of hydrophobically attached inner foulants were revealed by the SDS desorption. Resulted solutions for both HA and FA showed acidic nature for hydrophobically attached inner foulants, indicating protonated nature. Charge neutralization by protonation may facilitate intermolecular hydrophobic interactions (e.g., CH-π, π-π, van der Waals) among surface adhered foulants (Fig. 6) which can be readily desorbed with SDS. Decreased DOC_f content compared to DOC_i for SDS desorption solutions provide evidence for its sorption on AEM. Partially restored membranes after FA desorption facilitated enhanced SDS sorption, as evident from intensities of SDS features from vibrational data and SEM in Fig. 5. Overall, the pH variations among NaCl and SDS solutions suggest inner reversible HA foulants are protonated to a higher extent than partially protonated inner reversible FA foulants.

3.2.4. Postulated membrane fouling mechanisms

The desorption data, along with the EDR data, allowed postulation of three-step AEM fouling mechanisms (Fig. 6) by HS extracted from Northcentral province, Sri Lanka. Accordingly, the first phase includes initial electrostatic interactions between HA or FA and the AEM facilitated accumulation of foulants on the membrane. The negative surface charge of foulants due to carboxylate and phenolate groups appears to reduce by protons abstracted from water splitting. This process allows the stabilization of foulants on the membrane surface, first by reducing electrostatic repulsion among foulants and secondly, by facilitating inter-molecular hydrophobic interactions. The accumulation of foulants is restricted by high electrostatic repulsion inherited by FA due to high negative potential, which could be unable to be neutralized by protons from water splitting as for HA. As shown in Fig. 4e and 4.f the SEM data show comparatively higher coverage by HA foulant (29.58% coverage) compared to FA (27.23% coverage). Therefore, the second phase in which the accumulation of foulants on the surface is determined by the extent of neutralization of surface adhered foulants. SEM images show rather a high membrane surface coverage by HA; hence HA fouled membranes facilitate enhanced retention of organic moieties on the surface. Further, the stabilization of surface fouling by neutralization builds up a resistant to self-cleaning in EDR due to ineffective repulsion form electrode potential to the membrane foulants [23]. Third phase of fouling is the further stabilization of partially neutralized HS foulants by inter-molecular hydrophobic interactions. Future studies are required to determine the irreversible and/or reversible nature of these foulants.

Table 2
Summary of initial and final pH and DOC content in distilled water, 2% (w/w) NaCl and 0.5% (w/w) SDS as desorption solutions.

	Outer foulants				Inner foulants							
	Distilled water desorption				2% (w/w) NaCl desorption				0.5% (w/w) SDS desorption			
	pH_i	pH_f	DOC_i (mg/L)	DOC_f (mg/L)	pH_i	pH_f	DOC_i (mg/L)	DOC_f (mg/L)	pH_i	pH_f	DOC_i (mg/L)	DOC_f (mg/L)
HA-foulant	6.35 ± 0.03	6.45 ± 0.04	0.000 ± 0.000	2.863 ± 0.347	6.23 ± 0.02	5.49 ± 0.05	0.000 ± 0.000	0.564 ± 0.028	7.46 ± 0.04	6.99 ± 0.06	1967 ± 24.36	1259 ± 11.27
FA-foulant	6.35 ± 0.03	7.33 ± 0.03	0.000 ± 0.000	2.629 ± 0.326	6.23 ± 0.02	7.01 ± 0.04	0.000 ± 0.000	0.869 ± 0.069	7.46 ± 0.04	7.29 ± 0.05	1917 ± 17.31	1188 ± 16.31

pH_i- initial pH of the desorption solution
pH_f- final pH of the desorption solution
DOC_i- initial DOC content of the desorption solution
DOC_f- final DOC content of the desorption solution

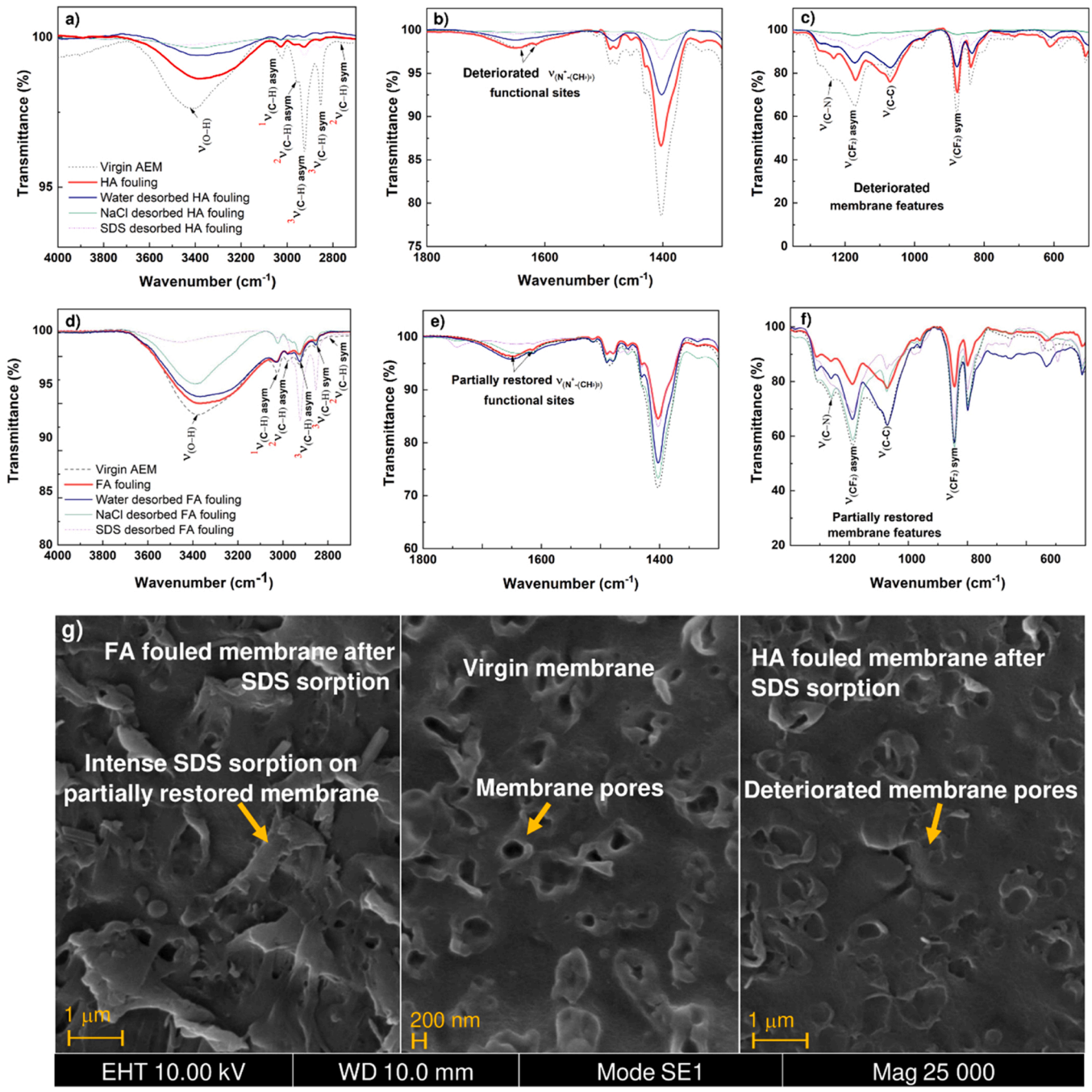

Fig. 5. : ATR-FTIR spectra comparing AEM surface functionality after subsequential removal of outer-most foulants by distilled water, and inner-most foulants by 2% (w/w) NaCl or 0.5% (w/w) SDS desorption. (a) High (ν, 4000–2700 cm^{-1}), (b) mid (ν, 1800–1300 cm^{-1}) and (c) low (ν, 1300–500 cm^{-1}) frequency spectral regions of HA fouled membranes. (d) High (ν, 4000–2700 cm^{-1}), (e) mid (ν, 1800–1300 cm^{-1}) and (f) low (ν, 1300–500 cm^{-1}) frequency spectral regions of FA fouled membranes. (g) SEM images to emphasize membrane deterioration by HA fouling after sequential removal of outer-foulants by DI water and inner-foulants by SDS.

4. Conclusions

The XPS, IR, and UV spectral information of groundwater humic and fulvic acids extracted from Northcentral province, Sri Lanka, have shown structural similarities. The aromaticity is higher for HA, while the aliphaticity is higher for FA. Compared to FA, HA is more hydrophobic. The degree of humification is less in Sri Lanka HS compared to IHSS. Relative abundance of COOH and phenolic OH are high for FA fraction, while the ester content was high for HA. Esterification seems to play an important role in migrating P, S, and Si in HA. Mechanistic steps of membrane fouling differ substantially between HA and FA, and ATR-FTIR data revealed significant membrane deterioration by HA. However, the HS-assisted membrane fouling mechanism can be explained in three steps; (i) initial electrostatic interactions, (ii) accumulation of foulants, and (iii) stabilization of the foulants is mainly due to sophisticated deviations that occurred in their COOH and phenolic OH contents.

CRediT authorship contribution statement

M. A. C. K. Hansima: Data curation, formal analysis, investigation, writing – original draft. **A.T Jayaweera**: Methodology, reviewing, and editing. **J. Ketharani**: Methododlogy, reviewing, and editing. **Tharindu Ritigala**: Methododlogy, resources. **Libing Zheng**: Methodology,

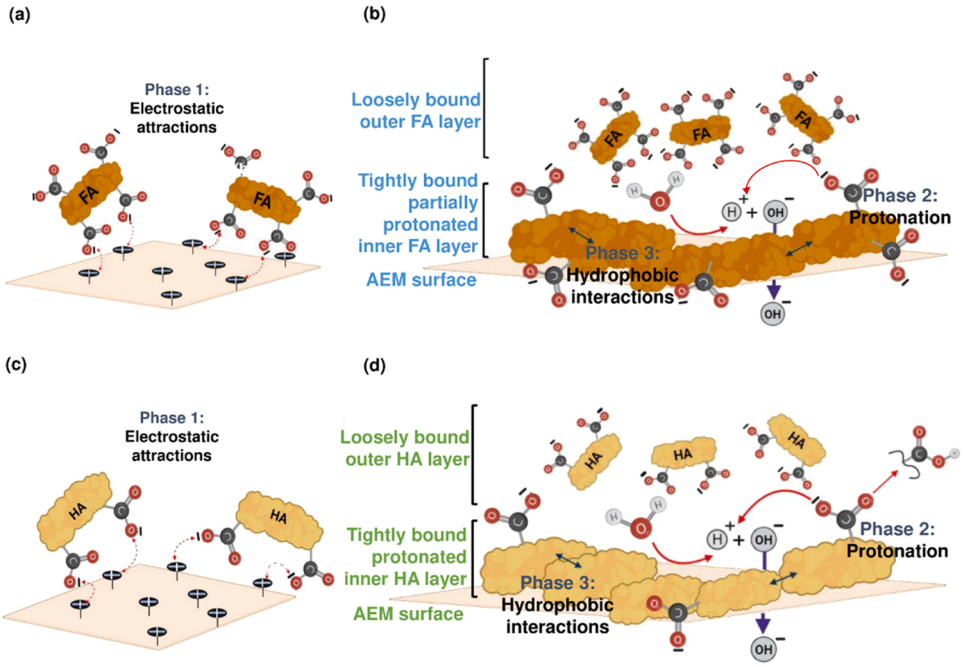

Fig. 6. Three-step membrane fouling mechanisms illustrating phase-1 electrostatic interactions of c) FA, e) HA, and phase-2 protonation and phase-3 hydrophobic interactions of d) FA, and f) HA.

resources. **D. R. Samarajeewa**: Supervision, reviewing, and editing. **K. G. N. Nanayakkara**: Supervision, reviewing, and editing. **Ajith C. Herath**: Supervision, reviewing, and editing. **Madhubhashini Makehelwala**: Conceptualization, validation. **K. B. S. N. Jinadasa:** Project administration, investigation, funding acquisition, reviewing. **S. K. Weragoda:** Supervision, reviewing and editing. **Yuansong Wei**: Supervision, reviewing and editing. **Rohan Weerasooriya:** Supervision, validation, reviewing, and editing.

Declaration of Competing Interest

The authors declare that they have no known competing financial interests or personal relationships that could have appeared to influence the work reported in this paper.

Acknowledgements

We acknowledge the financial support from the Joint Research Program of the National Science Foundation of Sri Lanka (ICRP/NSF-NSFC/2019/BS/03) and the National Natural Science Foundation of China (21861142020). Reviewers careful comments significantly enhanced manuscript quality.

Appendix A. Supporting information

Supplementary data associated with this article can be found in the online version at doi:10.1016/j.jece.2022.107456.

References

[1] J. Adusei-Gyamfi, B. Ouddane, L. Rietveld, J.P. Cornard, J. Criquet, Natural organic matter-cations complexation and its impact on water treatment: a critical review, Water Res. 160 (2019) 130–147, https://doi.org/10.1016/j.watres.2019.05.064.

[2] J.S. Gaffney, N.A. Marley, S.B. Clark, Humic and fulvic acids and organic colloidal materials in the environment, ACS Symp. Ser. 651 (1996) 2–16, https://doi.org/10.1021/bk-1996-0651.ch001.

[3] R. Vasilevich, E. Lodygin, V. Beznosikov, E. Abakumov, Molecular composition of raw peat and humic substances from permafrost peat soils of European Northeast Russia as climate change markers, Sci. Total Environ. 615 (2018) 1229–1238, https://doi.org/10.1016/j.scitotenv.2017.10.053.

[4] V.M. Semenov, A.S. Tulina, N.A. Semenova, L.A. Ivannikova, Humification and nonhumification pathways of the organic matter stabilization in soil: a review, Eurasia Soil Sci. 46 (4) (2013) 355–368, https://doi.org/10.1134/S106422931304011X.

[5] Z. He, T. Ohno, B. Cade-Menun, M. Erich, C. Honeycutt, Spectral and chemical characterization of phosphates associated with humic substances, Soil Sci. Soc. Am. J. 70 (. 2006) 1741–1751, https://doi.org/10.2136/sssaj2006.0030.

[6] O. Urrutia, et al., Physico-chemical characterization of humic-metal-phosphate complexes and their potential application to the manufacture of new types of phosphate-based fertilizers, J. Plant Nutr. Soil Sci. 177 (2) (2014) 800, https://doi.org/10.1002/jpln.201200651.

[7] R. Baigorri, J. Erro, Ó. Urrutia, J.M. Martinez, M. Mandado, M. Martín-Pastor, J. M. García-Mina, Both chemical and crystalline phase configuration influence the molecular features of humic acids in humic-calcium-phosphates fertilizers, RSC Adv. 9 (44) (2019) 25790–25796, https://doi.org/10.1039/c9ra04383g.

[8] Y. Lei, B. Song, M. Saakes, R.D. van der Weijden, C.J.N. Buisman, Interaction of calcium, phosphorus and natural organic matter in electrochemical recovery of phosphate, Water Res. 142 (2018) 10–17, https://doi.org/10.1016/j.watres.2018.05.035.

[9] N.A. Marley, P. Bennett, D.R. Janecky, J.S. Gaffney, Spectroscopic evidence for organic diacid complexation with dissolved silica in aqueous systems—I. Oxalic acid, Org. Geochem. 14 (5) (1989) 525–528, https://doi.org/10.1016/0146-6380(89)90032-6.

[10] M. Makehelwala, Y. Wei, S.K. Weragoda, R. Weerasooriya, Ca^{2+} and SO_4^{2-} interactions with dissolved organic matter: Implications of groundwater quality for CKDu incidence in Sri Lanka, J. Environ. Sci. 88 (2020) 326–337, https://doi.org/10.1016/j.jes.2019.09.018.

[11] R.L. Malcolm, Variations between humic substances isolated from soils, stream waters, and groundwaters as revealed by ^{13}C NMR spectroscopy, Humic Subst. Soil Crop Sci.: Sel. Read. (2015) 13–35, https://doi.org/10.2136/1990.humicsubstances.c2.

[12] J.B. Christensen, D.L. Jensen, C. Grøn, Z. Filip, T.H. Christensen, Characterization of the dissolved organic carbon in landfill leachate-polluted groundwater, Water Res. 32 (1) (1998) 125–135, https://doi.org/10.1016/S0043-1354(97)00202-9.

[13] J.J. Alberts, Z. Fulip, N. Hertkorn, Fulvic and humic acids isolated from groundwater: compositional characteristics and cation binding, J. Contam. Hydrol. 11 (3) (1992) 317–330, https://doi.org/10.1016/0169-7722(92)90022-7.

[14] C. Grøn, L. Wassenaar, M. Krog, Origin and structures of groundwater humic substances from three Danish aquifers, Environ. Int. 22 (5) (1996) 519–534, https://doi.org/10.1016/0160-4120(96)00056-6.

[15] J.I. Kim, G. Buckau, G.H. Li, H. Duschner, N. Psarros, Characterization of humic and fulvic acids from Gorleben groundwater, Fresenius' J. Anal. Chem. 338 (3) (1990) 245–252, https://doi.org/10.1007/BF00323017.

[16] S.V.R. Weerasooriya, C.B. Dissanayake, Modeling the nitrosation kinetics in simulated natural environmental conditions, Toxicol. Environ. Chem. 36 (3–4) (1992) 131–137, https://doi.org/10.1080/02772249209357836.

[17] M. Makehelwala, Y. Wei, S.K. Weragoda, R. Weerasooriya, L. Zheng, Characterization of dissolved organic carbon in shallow groundwater of chronic kidney disease affected regions in Sri Lanka, Sci. Total Environ. 660 (2019) 865–875, https://doi.org/10.1016/j.scitotenv.2018.12.435.

[18] T. Thayalakumaran, M.J. Lenahan, K.L. Bristow, Dissolved organic carbon in groundwater overlain by irrigated sugarcane, Groundwater 53 (4) (2015) 525–530, https://doi.org/10.1111/gwat.12258.
[19] S. Lee, J.S. Choi, C.H. Lee, Behaviors of dissolved organic matter in membrane desalination, Desalination 238 (1–3) (2009) 109–116, https://doi.org/10.1016/j.desal.2008.01.041.
[20] M. Hansima, M. Makehelwala, K. Jinadasa, Y. Wei, K. Nanayakkara, A.C. Herath, R. Weerasooriya, Fouling of ion exchange membranes used in the electrodialysis reversal advanced water treatment: a review, Chemosphere 263 (2021), 127951, https://doi.org/10.1016/j.chemosphere.2020.127951.
[21] A. Maartens, P. Swart, E.P. Jacobs, Humic membrane foulants in natural brown water: characterization and removal, Desalination 115 (3) (1998) 215–227, https://doi.org/10.1016/S0011-9164(98)00041-1.
[22] R. Chandrajith, C.B. Dissanayake, T. Ariyarathna, H.M.J.M.K. Herath, J. P. Padmasiri, Dose-dependent Na and Ca in fluoride-rich drinking water —Another major cause of chronic renal failure in tropical arid regions, Sci. Total Environ. 409 (4) (2011) 671–675, https://doi.org/10.1016/j.scitotenv.2010.10.046.
[23] M.A.C.K. Hansima, J. Ketharani, D.R. Samarajeewa, K. Nanayakkara, A.C. Herath, M. Makehelwala, S. Indika, K. Jinadasa, S.K. Weragoda, Y. Wei, R. Weerasooriya, Probing fouling mechanism of anion exchange membranes used in electrodialysis self-reversible treatment by humic acid and calcium ions, Chem. Eng. J. Adv. 8 (2021), 100173, https://doi.org/10.1016/j.ceja.2021.100173.
[24] M. Haddad, S. Mikhaylin, L. Bazinet, O. Savadogo, J. Paris, Electrochemical acidification of Kraft black liquor by electrodialysis with bipolar membrane: ion exchange membrane fouling identification and mechanisms, J. Colloid Interface Sci. 488 (2017) 39–47, https://doi.org/10.1016/j.jcis.2016.10.015.
[25] M. Persico, S. Mikhaylin, A. Doyen, L. Firdaous, R. Hammami, M. Chevalier, C. Flahaut, P. Dhulster, L. Bazinet, Formation of peptide layers and adsorption mechanisms on a negatively charged cation-exchange membrane, J. Colloid Interface Sci. 508 (2017) 488–499, https://doi.org/10.1016/j.jcis.2017.08.029.
[26] M. Persico, S. Mikhaylin, A. Doyen, L. Firdaous, V. Nikonenko, N. Pismenskaya, L. Bazinet, Prevention of peptide fouling on ion-exchange membranes during electrodialysis in overlimiting conditions, J. Membr. Sci. 543 (2017) 212–221, https://doi.org/10.1016/j.memsci.2017.08.039.
[27] L.E. Bacher, C. de Oliveira, A. Giacobbo, T. Benvenuti, A.B. Lacerda, A. M. Bernardes, M. Rodrigues, Coupling coagulation using tannin-based product with electrodialysis reversal to water treatment: a case study, J. Environ. Chem. Eng. 5 (6) (2017) 6008–6015, https://doi.org/10.1016/j.jece.2017.11.002.
[28] H.-J. Lee, J.-H. Choi, J. Cho, S.-H. Moon, Characterization of anion exchange membranes fouled with humate during electrodialysis, J. Membr. Sci. 203 (1) (2002) 115–126, https://doi.org/10.1016/S0376-7388(01)00792-X.
[29] L. Shi, S. Xie, Z. Hu, G. Wu, L. Morrison, P. Croot, H. Hu, X. Zhan, Nutrient recovery from pig manure digestate using electrodialysis reversal: membrane fouling and feasibility of long-term operation, J. Membr. Sci. 573 (2019) 560–569, https://doi.org/10.1016/j.memsci.2018.12.037.
[30] V. Lindstrand, G. Sundström, A.-S. Jönsson, Fouling of electrodialysis membranes by organic substances, Desalination 128 (1) (2000) 91–102, https://doi.org/10.1016/S0011-9164(00)00026-6.
[31] B. de Jaegher, E. Larumbe, W. de Schepper, A. Verliefde, I. Nopens, Data on ion-exchange membrane fouling by humic acid during electrodialysis, Data Brief. 31 (2020), 105763, https://doi.org/10.1016/j.dib.2020.105763.
[32] E.M. Thurman, Organic geochemistry of natural waters, Org. Geochem. Nat. Waters (1985), https://doi.org/10.1007/978-94-009-5095-5.
[33] S. Valencia, J.M. Marín, G. Restrepo, F.H. Frimmel, Application of excitation-emission fluorescence matrices and UV/Vis absorption to monitoring the photocatalytic degradation of commercial humic acid, Sci. Total Environ. 442 (2013) 207–214, https://doi.org/10.1016/j.scitotenv.2012.10.058.
[34] H. Niu, H. Yang, L. Tong, S. Zhong, Y. Liu, Spectral study of humic substance extract from pressurized oxidizing slag of Carlin-typed gold deposit, in, J. Phys.: Conf. Ser. 1347 (1) (2019), 012027, https://doi.org/10.1088/1742-6596/1347/1/012027.
[35] M. Fuentes, G. González-Gaitano, J.M. García-Mina, The usefulness of UV–visible and fluorescence spectroscopies to study the chemical nature of humic substances from soils and composts, Org. Geochem. 37 (12) (2006) 1949–1959, https://doi.org/10.1016/j.orggeochem.2006.07.024.
[36] T. Tanaka, S. Nagao, H. Ogawa, Attenuated total reflection fourier transform infrared (ATR-FTIR) spectroscopy of functional groups of humic acid dissolving in aqueous solution, Anal. Sci. 17 (2001) i1081–i1084.
[37] F. Monteil-Rivera, E.B. Brouwer, S. Masset, Y. Deslandes, J. Dumonceau, Combination of X-ray photoelectron and solid-state 13C nuclear magnetic resonance spectroscopy in the structural characterisation of humic acids, Anal. Chim. Acta 424 (2) (2000) 243–255, https://doi.org/10.1016/S0003-2670(00)01139-9.
[38] L. Doskočil, J. Burdíková-Szewieczková, V. Enev, L. Kalina, J. Wasserbauer, Spectral characterization and comparison of humic acids isolated from some European lignites, Fuel 213 (2018) 123–132, https://doi.org/10.1016/j.fuel.2017.10.114.
[39] J. Song, P. Peng, Surface characterization of aerosol particles in Guangzhou, China: A study by XPS, Aerosol Sci. Technol. 43 (12) (2009) 1230–1242, https://doi.org/10.1080/02786820903325394.
[40] J.R. Araujo, B.S. Archanjo, K.R. de Souza, W. Kwapinski, N. Falcão, E.H. Novotny, C.A. Achete, Selective extraction of humic acids from an anthropogenic Amazonian dark earth and from a chemically oxidized charcoal, Biol. Fertil. Soils 50 (8) (2014) 1223–1232, https://doi.org/10.1007/s00374-014-0940-9.
[41] T. Abe, A. Watanabe, X-ray photoelectron spectroscopy of nitrogen functional groups in soil humic acids, Soil Sci. 169 (1) (2004) 35–43, https://doi.org/10.1097/01.ss.0000112016.97541.28.
[42] D.B. Zandonadi, C.R.R. Matos, R.N. Castro, R. Spaccini, F.L. Olivares, L.P. Canellas, Alkamides: a new class of plant growth regulators linked to humic acid bioactivity, Chem. Biol. Technol. Agric. 6 (1) (2019) 23, https://doi.org/10.1186/s40538-019-0161-4.
[43] A. Gulkowska, M. Krauss, D. Rentsch, J. Hollender, Reactions of a sulfonamide antimicrobial with model humic constituents: assessing pathways and stability of covalent bonding, Environ. Sci. Technol. 46 (4) (2012) 2102–2111, https://doi.org/10.1021/es202272w.
[44] J.A. Rice, P. MacCarthy, Statistical evaluation of the elemental composition of humic substances, Org. Geochem. 17 (5) (1991) 635–648, https://doi.org/10.1016/0146-6380(91)90006-6.
[45] Z. Fu, F. Wu, K. Song, Y. Lin, Y. Bai, Y. Zhu, J.P. Giesy, Competitive interaction between soil-derived humic acid and phosphate on goethite, Appl. Geochem. 36 (2013) 125–131, https://doi.org/10.1016/j.apgeochem.2013.05.015.
[46] S.D. Rosan, C.A. Silva, H.J.G.M. Maluf, Humic acid-phosphate fertilizer interaction and extractable phosphorus in soils of contrasting texture, Rev. Cienc. Agron. 49 (1) (2018), https://doi.org/10.5935/1806-6690.20180004.
[47] J. Fatema, S. Bhattacharjee, D. Pernitsky, A. Maiti, study of the aggregation behavior of silica and dissolved organic matter in oil sands produced water using Taguchi experimental design, Energy Fuels 29 (11) (2015) 7465–7473, https://doi.org/10.1021/acs.energyfuels.5b01223.
[48] M.A. Olivella, J.C. del Ríío, J. Palacios, M.A. Vairavamurthy, F.X.C. de las Heras, Characterization of humic acid from leonardite coal: an integrated study of PY-GC-MS, XPS and XANES techniques, J. Anal. Appl. Pyrolysis 63 (1) (2002) 59–68, https://doi.org/10.1016/S0165-2370(01)00141-3.
[49] G. v Korshin, C.W. Li, M.M. Benjamin, Monitoring the properties of natural organic matter through UV spectroscopy: a consistent theory, Water Res. 31 (7) (1997) 1787–1795, 10.1016/S0043-1354(97)00006-7.
[50] C.S. Uyguner, M. Bekbolet, Evaluation of humic acid photocatalytic degradation by UV–vis and fluorescence spectroscopy (SPEC. ISS), Catal. Today 101 (3–4) (2005) 267–274, https://doi.org/10.1016/j.cattod.2005.03.011.
[51] C. Wang, X. Zhang, J. Wang, C. Chen, Characterization of dissolved organic matter as N-nitrosamine precursors based on hydrophobicity, molecular weight and fluorescence, J. Environ. Sci. 25 (1) (2013) 85–95, https://doi.org/10.1016/S1001-0742(12)60029-1.
[52] O. Yakimenko, D. Khundzhua, A. Izosimov, V. Yuzhakov, S. Patsaeva, Source indicator of commercial humic products: UV-Vis and fluorescence proxies, J. Soils Sediment. 18 (4) (2018) 1279–1291, https://doi.org/10.1007/s11368-016-1528-9.
[53] J. Peuravuori, K. Pihlaja, Molecular size distribution and spectroscopic properties of aquatic humic substances, Anal. Chim. Acta 337 (2) (1997) 133–149, https://doi.org/10.1016/S0003-2670(96)00412-6.
[54] Y. Wang, Z. Zhang, C. Jiang, T. Xu, Electrodialysis process for the recycling and concentrating of tetramethylammonium hydroxide (TMAH) from photoresist developer wastewater, Ind. Eng. Chem. Res. 52 (51) (2013) 18356–18361, https://doi.org/10.1021/ie4023995.
[55] J. Zhou, H. Kuang, W. Zhuang, Y. Chen, D. Liu, H. Ying, J. Wu, Application of electrodialysis to extract 5′-ribonucleotides from hydrolysate: efficient decolorization and membrane fouling, RSC Adv. 8 (51) (2018) 29115–29128, https://doi.org/10.1039/c8ra02550a.
[56] M. Bdiri, V. Perreault, S. Mikhaylin, C. Larchet, F. Hellal, L. Bazinet, L. Dammak, Identification of phenolic compounds and their fouling mechanisms in ion-exchange membranes used at an industrial scale for wine tartaric stabilization by electrodialysis, Sep. Purif. Technol. 233 (2020), 115995, https://doi.org/10.1016/j.seppur.2019.115995.
[57] M. Sanchez-Camazano, M.J. Sanchez-Martin, M.S. Rodriguez-Cruz, Sodium dodecyl sulphate-enhanced desorption of atrazine: effect of surfactant concentration and of organic matter content of soils, Chemosphere 41 (8) (2000) 1301–1305, https://doi.org/10.1016/S0045-6535(99)00503-2.